UNSW SYDNEY

Groundwater constraints on simulated transpiration variability over Southeastern Australian forests

Author:
Decker, Mark; Pitman, Andrew; Evans, Jason

Publication details:
Journal of Hydrometeorology
v. 14
Chapter No. 2
pp. 543-559

Publication Date:
2013

Publisher DOI:
http://dx.doi.org/10.1175/JHM-D-12-058.1

License:
https://creativecommons.org/licenses/by-nc-nd/3.0/au/
Link to license to see what you are allowed to do with this resource.

Downloaded from http://hdl.handle.net/1959.4/53693 in https://unsworks.unsw.edu.au on 2024-04-17

Groundwater Constraints on Simulated Transpiration Variability over Southeastern Australian Forests

M. DECKER

Climate Change Research Centre, University of New South Wales, Sydney, New South Wales, Australia

A. J. PITMAN

ARC Centre of Excellence for Climate System Science, University of New South Wales, Sydney, New South Wales, Australia

J. P. EVANS

Climate Change Research Centre, University of New South Wales, Sydney, New South Wales, Australia

(Manuscript received 21 April 2012, in final form 14 October 2012)

ABSTRACT

A land surface scheme with and without groundwater–vegetation interactions is used to explore the impact of rainfall variability on transpiration over drought-vulnerable regions of southeastern Australia. The authors demonstrate that if groundwater is included in the simulations, there is a low correlation between rainfall variability and the response of transpiration to this variability over forested regions. Groundwater reduces near-surface water variability, enabling forests to maintain transpiration through several years of low rainfall, in agreement with independent observations of vegetation greenness. If groundwater is not included, the transpiration variability matches the rainfall variability independent of land cover type. The authors' results suggest that omitting groundwater in regions where groundwater sustains forests will 1) probably overestimate the likelihood of forest dieback during drought, 2) overestimate a positive feedback linked with declining transpiration and a drying boundary layer, and 3) underestimate the impact of land cover change due to inadequately simulating the different responses to drought for different land cover types.

1. Introduction

Southeastern (SE) Australia has recently recovered from a long and intense drought that caused observable reductions in both groundwater (van Dijk et al. 2011) and surface water stores (Cai et al. 2009; Leblanc et al. 2009). While long-term droughts in Australia, caused in part by variability in the Indian Ocean sea surface temperatures (Ummenhofer et al. 2009), can last a decade or longer, forests dominated by the genus *Eucalyptus* flourish over significant parts of SE Australia.

While dieback associated with severe drought does occur, eucalypts have developed multiple strategies to withstand decadal-scale drought. There is substantial evidence that many eucalypts grow roots to depths exceeding 20 m, allowing them to tap deep soil water. This contrasts with more shallow-rooted species that are more vulnerable to drought (Rice et al. 2004). Schenk and Jackson (2002) report *Eucalyptus marginata* growing roots to 15–18 m and suggest that the deepest roots should be found in environments with deep soil moisture and a dry season. Eberbach and Burrows (2006) show that transpiration from a dominant eucalypt species in SE Australia responded only slightly to drought, while more shallowly rooted species had larger responses. O'Grady et al. (1999) found two dominant species of eucalypts in tropical Australia increasing transpiration in the dry season because of the increased evaporative demand and because the trees could access groundwater. O'Grady et al. (2006) also found dry tropical woodlands in Queensland to be utilizing groundwater. Additionally, Yang et al. (2011) recently demonstrated a sensitivity of transpiration from *Eucalyptus populnea*

Corresponding author address: Mark Decker, Climate Change Research Centre, Level 4 Mathews Building, University of New South Wales, Sydney, NSW 2052, Australia.
E-mail: m.decker@unsw.edu.au

DOI: 10.1175/JHM-D-12-058.1

© 2013 American Meteorological Society

to human manipulation of groundwater levels, suggesting that these ecosystems are also dependent on groundwater. Similarly, tree plantations in SE Australia have been shown to impact groundwater, demonstrating the link between vegetation and groundwater (Benyon et al. 2006). Overall, there is a strong view that many Australian *Eucalyptus* ecosystems are dependent on groundwater interactions (Eamus and Froend 2006).

Despite evidence that many Australian ecosystems are dependent on groundwater (Eamus and Froend 2006), these interactions are omitted from almost all global and regional climate modeling research focused on how transpiration responds to drought events. However, research addressing these interactions has become more prevalent following several recent studies (York et al. 2002; Anyah et al. 2007; Miguez-Macho et al. 2007) that have demonstrated the role that groundwater plays in maintaining evapotranspiration during dry periods. Over the last 10 years, land surface model (LSM) development has seen the inclusion of groundwater components (Liang et al. 2003; Yeh and Eltahir 2005; Fan et al. 2007; Niu et al. 2007; Oleson et al. 2008; Rosero et al. 2009; Decker and Zeng 2009; Yeh and Famiglietti 2009; Maxwell et al. 2011), resulting in improved simulations of the hydrological cycle in offline experiments. This model development is particularly important given that groundwater dynamics also significantly affect soil moisture, land surface fluxes, and convective precipitation in fully coupled simulations (Seuffert et al. 2002; Anyah et al. 2007; Maxwell et al. 2007; Miguez-Macho et al. 2007; Leung et al. 2011). The addition of groundwater dynamics in LSMs has been achieved with varying degrees of complexity, including fully three-dimensional groundwater models, a deeper soil column, a simple coupled groundwater model, or via an appropriate boundary condition at the bottom of the soil column (Gulden et al. 2007; Kollet and Maxwell 2008; Decker and Zeng 2009).

Given the adaptation of eucalypts to drought and previous research that has demonstrated the importance of groundwater–vegetation interactions in semiarid regions, we hypothesize that groundwater–vegetation interactions play an important role in sustaining transpiration over forests in SE Australia through periods of low rainfall. We use an LSM forced with observationally corrected atmospheric forcing data together with two satellite-derived metrics of vegetation to assess how significantly the inclusion of groundwater affects the variability of simulated transpiration during the recent SE Australian drought. We focus on transpiration because this flux is intimately associated with photosynthesis, net primary productivity, and the capacity of trees to withstand drought. Our goal is to determine whether including groundwater is necessary in simulations of land–atmosphere interactions over SE Australia by evaluating the simulated transpiration response to drought using the observed vegetation response over various different vegetation types.

2. Methodology

a. Model configuration and experiments

We use the Community Land Model version 4 (CLM4) to simulate the land surface (Oleson et al. 2010). CLM4, a one-dimensional water and energy balance land surface model, is the land surface component in the National Center for Atmospheric Research (NCAR) Community Earth System Model (CESM), which is a comprehensive Earth system model [previously referred to as the Community Climate System Model (CCSM); Gent et al. 2011]. CLM4 has been widely used to study the hydrological cycle, energy balance, vegetation dynamics, and biogeochemical fluxes at the land surface (Gotangco Castillo et al. 2012; Lawrence et al. 2012; Li et al. 2011; Sacks et al. 2009; Sakaguchi et al. 2011; Stöckli et al. 2008) and has also been utilized in differing ways to study aspects of groundwater (Gulden et al. 2007; Niu et al. 2007; Kollet and Maxwell 2008; Lo et al. 2008; Decker and Zeng 2009).

CLM4 calculates the surface fluxes on the basis of the Monin–Obhukov similarity theory using an energy balance approach. Separate fluxes (sensible and latent heat) are calculated for the different vegetation types (and nonvegetated regions including bare soil and lakes) in each grid cell and subsequently aggregated to the gridcell resolution. Transpiration (together with canopy and ground evaporation) is iteratively calculated alongside sensible heat, with sunlit and shaded leaves considered separately (Oleson et al. 2010). CLM4 determines transpiration from the rate of photosynthesis that is in part constrained by soil moisture. The dependence on soil moisture is determined by the soil matric potential (the force resulting from the capillary forces in the soil) in each soil layer, the root concentration (dependent on the predefined plant functional type), and the plant functional type dependence on water stress. The root concentration is highest approximately 10 cm from the surface and declines exponentially below this depth, with trees retaining a higher fraction of roots near the bottom of the soil column than other plant types. For grasses, ~99% of the roots are located within 1 m from the surface, while for broadleaf evergreen trees, ~90% of the roots are within this depth. This is broadly consistent with meta-analyses of global data on root distributions (Jackson et al. 1996; Canadell et al. 1996).

Soil water in CLM4 is simulated using 10 soil layers and a groundwater model consisting of an unconfined aquifer below the 10 soil layers. The aquifer is not constrained to a specific depth, while the thickness of the soil layers varies exponentially, with the top layer ~17 mm thick and the 10th layer ~1.14 m thick. The resulting soil column extends from the surface to a depth of ~3.43 m. In the control (groundwater) simulations, herein referred to as GW, the default configuration of CLM4 (including the groundwater model) is used. The influence of the underlying aquifer on the calculation on the flux of water to and from the bottom (10th) soil layer and on the recharge rate is removed in the simulation without groundwater (referred to as NGW).

The groundwater component in CLM4 consists of an unconfined aquifer beneath the 10 soil layers. The change in groundwater at each time step is given by

$$W_{t_{n+1}} = W_{t_n} + (q_{\text{recharge}} - q_{\text{dri}})\Delta t, \tag{1}$$

where $W_{t_{n+1}}$ and W_{t_n} are the amount of water in the aquifer (mm) at time $n + 1$ and time n, q_{recharge} (mm s^{-1}) is the recharge rate of the aquifer, q_{drai} (mm s^{-1}) is the subsurface drainage, and Δt is the time step (s). The subsurface drainage in CLM4 is defined as the runoff that originates from within the soil column and is calculated as a function of the water table depth. The recharge rate (mm s^{-1}) is calculated as

$$q_{\text{recharge}} = \frac{\Delta\theta_{\text{nlev}}(Z_{\text{wtd}} - Z_{h,\text{nlev}})}{\Delta t}, \tag{2}$$

where $\Delta\theta_{\text{nlev}}$ is the change in soil water in the bottom (10th) soil layer (mm^3 mm^{-3}), and Z_{wtd} ($Z_{h,\text{nlev}}$) is the depth of the water table (bottom of the 10th soil layer) in millimeters.

When the water table depth is located within the soil column, no water flows vertically from the soil column to the aquifer. When the water table depth is beneath the soil column, the flux to/from the aquifer is given by

$$\begin{aligned} q_{\text{out}} &= -k\frac{\partial(\psi - \psi^E)}{\partial z} \\ &= -k_{\text{nlev}}\left[\frac{\psi_{\text{nlev}+1} - \psi_{\text{nlev}}}{z_{\text{wtd}} - z_{\text{nlev}}} - \frac{\psi^E_{\text{nlev}+1} - \psi^E_{\text{nlev}}}{z_{\text{wtd}} - z_{\text{nlev}}}\right], \end{aligned} \tag{3}$$

where q_{out} is the flux (mm s^{-1}), k_{nlev} is the hydraulic conductivity (mm s^{-1}) between the aquifer and the bottom (10th) soil layer, $\psi_{\text{nlev}+1}$ (ψ_{nlev}) is the soil matric potential of the aquifer (bottom soil layer) in millimeters, and $\psi^E_{\text{nlev}+1}$ (ψ^E_{nlev}) is the equilibrium soil matricpotential of the aquifer (bottom soil layer) in millimeters. The use of $\psi^E_{\text{nlev}+1}$ and ψ^E_{nlev} is necessary to prevent erroneous water movement in variably saturated soils (Zeng and Decker 2009). Equation (3) controls the vertical movement of water out of the bottom soil layer, directly contributing to $\Delta\theta_{\text{nlev}}$, which in turn determines the recharge rate through Eq. (2). The GW simulations use the full CLM4 hydrology scheme, including Eqs. (1)–(3).

The NGW simulations remove any influence of the aquifer on the soil moisture by modifying Eq. (3) as

$$q_{\text{out}} = -k\frac{\partial(\psi - \psi^E)}{\partial z} = -k_{\text{nlev}}. \tag{4}$$

Equation (4) removes the influence that the aquifer exerts on the soil moisture by removing the soil matric potential of the aquifer from Eq. (3). To ensure that the aquifer cannot transfer water to the bottom layer, Eq. (2) is also modified as

$$q_{\text{recharge}} = \max\left[0.0, \frac{\Delta\theta_{\text{nlev}}(Z_{\text{wtd}} - Z_{h,\text{nlev}})}{\Delta t}\right]. \tag{5}$$

Using Eqs. (4) and (5) results in a free drainage bottom boundary condition so that the aquifer does not influence fluxes at the bottom of the soil column in the NGW runs, and water is prevented from flowing from the aquifer to the soil column. The water table depth in CLM4 is calculated diagnostically on the basis of the water content of the soil layers and the aquifer. Therefore, the water table is simply a reflection of the total column moisture in the model, varying spatially and temporally with the total column moisture. Equations (4) and (5) alter how the flux of water between the surface and the aquifer are calculated; however, the amount of water in the aquifer still varies temporally since the aquifer is left in the model (and not removed completely). Therefore, the calculation of the water table depth (or other properties that depend on the water table depth, such as surface and subsurface runoff) does not need to be modified for the NGW simulation even though the dynamics of the aquifer will differ between the GW and NGW simulations.

All simulations are initialized with the default CLM4 initial conditions and spun up using corrected National Centers for Environmental Prediction (NCEP)–NCAR reanalysis (Qian et al. 2006) data interpolated to 0.25° × 0.25° for the period 1948–79, at a horizontal resolution of 0.25° × 0.25° over Australia. Static land cover and vegetation fractions with leaf and stem area indices (LAI and SAI, respectively) specified from monthly varying Moderate Resolution Imaging Spectroradiometer (MODIS) data are used. Observed LAI is chosen

in this study over the prognostic LAI available in CLM4 in order to isolate the effect of groundwater on transpiration. Using a prescribed LAI (with dynamic phenology and vegetation in CLM4 turned off) removes the influence of dynamic phenology on the land surface fluxes, allowing only the influence of groundwater to be documented. Restart files from 1979 were then used to simulate the period from 1979 to 2009, with the analysis covering the period coincident with the satellite observations (2002–09).

b. Forcing data

Land surface model simulations have been shown to be sensitive to biases in forcing data (Robock et al. 2003), and scaling precipitation forcing to match observations can result in much improved land model simulations (Pan et al. 2003). To this end, the forcing data used to drive the LSM from 1979 to 2009 consist of a combination of the Modern-Era Retrospective Analysis for Research and Applications (MERRA) reanalysis (Rienecker et al. 2011) and the Bureau of Meteorology Australian Water Availability Project (BAWAP) gridded daily precipitation data spanning the period 1900 to the present (Jones et al. 2009). MERRA is a global reanalysis product covering 1979 to the present with an hourly temporal resolution on a ½° × ⅔° grid, and BAWAP is a gauge-based gridded observation product with daily temporal resolution on a 0.05° × 0.05° grid. To facilitate simulations at a quarter degree resolution, the forcing datasets were interpolated to 0.25° × 0.25° using a mass conservative scheme. While the corrected NCEP–NCAR reanalysis is used to spin up the model (because of availability prior to 1979), the MERRA reanalysis product is chosen as the primary source of forcing data because of its high spatial resolution and accuracy (Decker et al. 2012; Reichle et al. 2011; Yi et al. 2011).

We take the BAWAP precipitation as the ground truth in this study because of the proven accuracy of BAWAP and the high number of observation stations (greater than 6000 for the period 2000–09) used over SE Australia (Jones et al. 2009). Evaluation of the MERRA precipitation using BAWAP reveals large differences between the two datasets. Figure 1a shows the spatially averaged interannual precipitation anomalies for MERRA and BAWAP over SE Australia (defined in this study as 27°S–40°S and 140°E–155°E). From Fig. 1a it is clear that the large negative precipitation anomalies in BAWAP around 2002 and 2006 are well captured in MERRA. However, the mean precipitation rate in MERRA (Fig. 1c) is much lower than from BAWAP over many forested regions (the hatched area in Fig. 1c). The underestimation of precipitation in MERRA over the forested regions in SE Australia is problematic for our simulations since this region shows significant sensitivity to groundwater–surface water interactions (see section 3).

To mitigate the issues caused by the inaccuracies in the MERRA precipitation data, the MERRA precipitation is scaled using the BAWAP observations in a similar manner to those proposed by Qian et al. (2006) and Berg et al. (2003). The correction method scales the MERRA precipitation data at each time step and grid point:

$$P^{S}_{i,j} = \frac{\overline{P}^{B}_{j}}{\overline{P}^{M}_{j}} P^{M}_{i,j}, \tag{6}$$

where $P^{S}_{i,j}$ is the scaled MERRA precipitation at (hourly) time step i of month j, $P^{M}_{i,j}$ is the uncorrected MERRA precipitation, $\overline{P}^{M}_{j}$ is the mean monthly precipitation from MERRA, and $\overline{P}^{B}_{j}$ is the monthly mean precipitation from BAWAP. Equation (6) is applied to each grid point after using a mass conservative scheme to interpolate both datasets to 0.25° × 0.25° resolution. The use of Eq. (6) ensures that the monthly precipitation bias (between MERRA and BAWAP) at each grid cell is removed from the corrected forcing. All other forcing variables (surface pressure, air temperature, wind speed, specific humidity, incoming solar radiation, and downward longwave radiation) use the uncorrected values from MERRA.

c. Observed soil moisture variability

The model simulations of total column water (including both the aquifer and the soil column) are validated against the Gravity Recover and Climate Experiment (GRACE) observations (Tapley et al. 2004). GRACE estimates the changes in total column moisture (including groundwater, soil water, canopy storage, and snow) indirectly by measuring the changes in Earth's gravitational field caused by the variations in terrestrial moisture. The release 05 and release 04 data (available from http://grace.jpl.nasa.gov/ and referred to here as GRACE5 and GRACE4, respectively) span 2004–10 and 2002–10, respectively, and are utilized in this study (Landerer and Swenson 2012). The primary difference between the two datasets is the level 2 spherical harmonic GRACE data used to derive the changes in terrestrial total water storage, with GRACE5 being the more accurate of the two. The total water storage change data have been filtered to remove the spatially correlated errors found in the raw GRACE observations, and the GRACE5 data have also been scaled to address the issues arising spatial smoothing (Landerer and Swenson 2012). The GRACE measurements are provided on a 1° × 1° grid; therefore, the model simulations

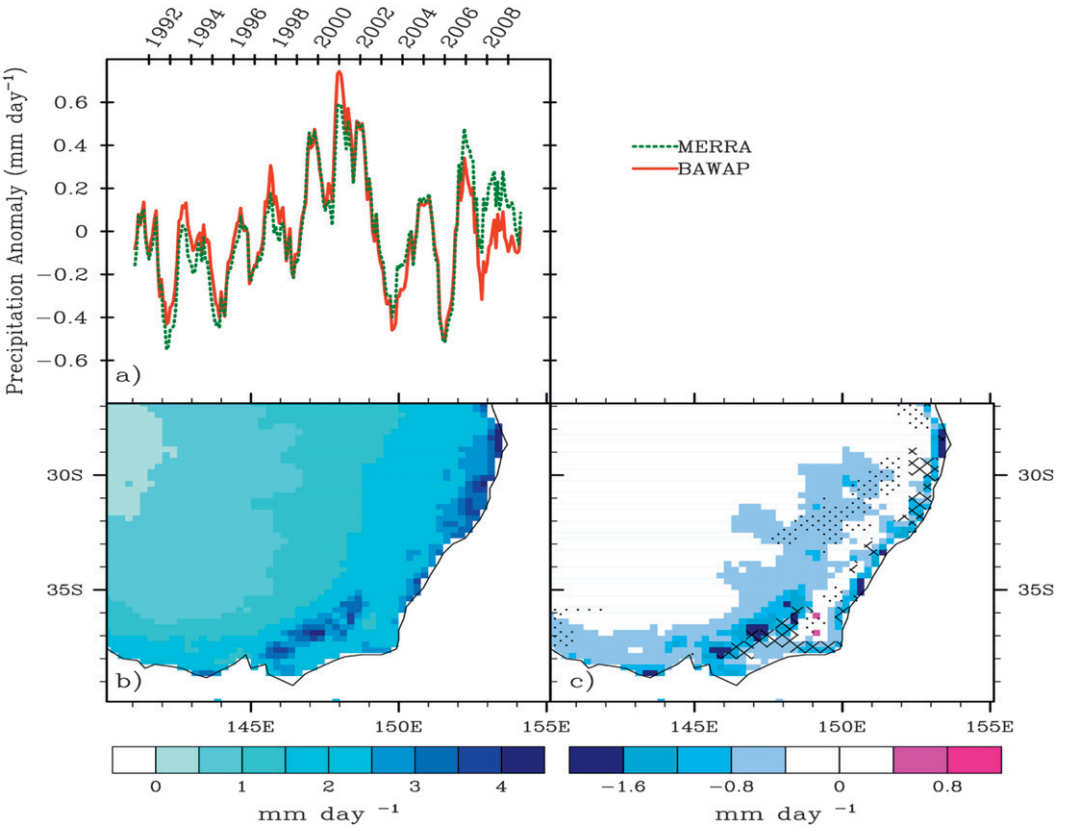

FIG. 1. (a) The spatially averaged deseasonalized (by removing the mean annual cycle) monthly precipitation rate (mm day^{-1}) for SE Australia (defined here as 27°S–40°S and 140°E–155°E) for the period from 1990 to 2009. (b) The mean precipitation rate (mm day^{-1}) from the same region as (a) for the period from 2002 to 2008 (the analysis period) for BAWAP. (c) The difference (MERRA − BAWAP) between the two datasets. The stippling in (c) shows grid cells covered by at least 60% grass, while the hatching denotes grid cells with at least 85% forest cover.

are aggregated to this resolution for the comparison. Various GRACE observations have been used extensively to validate the performance of land surface models (Ngo-Duc et al. 2007; Niu et al. 2007; Decker and Zeng 2009; Lo et al. 2010; Lawrence et al. 2012) as well as to examine changes in groundwater (Yeh et al. 2006; Leblanc et al. 2009).

d. Observed vegetation metrics

Two satellite-based vegetation metrics representative of plant greenness are used to evaluate the model. The photosynthetic vegetation fraction (PVF) estimates the fraction of a grid cell that is photosynthetically active and is used here in part because the data are developed using observations from various locations across Australia (Guerschman et al. 2009). The product utilizes the normalized difference vegetation index (NDVI) and bands 7 [shortwave infrared (SWIR)3] and 6 (SWIR2) from MODIS to derive the fraction of photosynthetic vegetation, the fraction of nonphotosynthetic vegetation, and the fraction of bare soil for a 0.05° × 0.05° grid at a temporal resolution of 8 days. The MODIS-derived fractions show good agreement with locally measured quantities with coefficient of determination (r^2) values ranging from about 0.6 to 0.9, depending on the location (Guerschman et al. 2009). The second product is a revised LAI from MODIS (MOD15A2) that has been filtered to remove erroneous values and filled to create a continuous time series (Yuan et al. 2011). The LAI is a similar measure to NDVI in that it varies roughly exponentially with NDVI for needleleaf and broadleaf forests (Buermann et al. 2002). Although derived and representative of different quantities (percent of a grid cell versus area of leaves per area of land surface), both products estimate the state of the vegetation with larger values over green, leaf-filled areas.

The physical basis for evaluating simulated transpiration through the use of satellite observed vegetation greenness metrics is based on the fact that both are directly related to gross primary production (GPP). Transpiration can be viewed as a cost of photosynthesis (Cowan 1982), while the level of vegetation greenness

is the result of the balance between leaf carbon gain (GPP) and loss (i.e., respiration and litter loss) of an ecosystem. Numerous processes alter the relationship between transpiration, photosynthesis, and vegetation greenness, with differing factors limiting leaf growth depending on the ecosystem considered (Cowling and Field 2003). Photosynthesis is dependent on the stomatal conductance, which is dependent on relative humidity and leaf CO_2 concentrations (McMurtrie et al. 1992). Photosynthesis is also dependent on the available radiation and radiation use efficiency, which itself is dependent on the plant type, nitrogen content of the leaves, temperature, and soil moisture (Sinclair and Horie 1989; Landsberg and Hingston 1996). Transpiration also depends on the vapor pressure deficit (with larger deficits leading to larger water fluxes), so that long-term transpiration over large scales can be viewed as a function of the product of net primary production (NPP) and vapor pressure deficit (Chen and Coughenour 2004). Despite the uncertainty inherent in comparing transpiration to satellite observations of the vegetative state, the NDVI has been shown to be well correlated ($r = 0.80$) with estimates of evapotranspiration in North American prairies (Szilagyi et al. 1998). Even with the annual cycle removed, NDVI explained the majority of the variance in these regions (Szilagyi et al. 1998). While satellite-derived evapotranspiration (ET) products could be used to evaluate the simulated ET, we are examining specifically how transpiration is affected by groundwater. It would be likely impossible to disentangle the transpiration component of the vegetation–ET relationship over the regions examined here. Further, these satellite ET products are derived and validated without using observations over Australia, where the vegetation is known to be different from the typical validation locations (Mu et al. 2007; Yuan et al. 2011; Zhang et al. 2010). Therefore, we use satellite-based measures of the state of the vegetation (LAI and PVF) as a proxy for evaluating the model simulations. Rather than directly comparing the vegetative state with the simulated transpiration, we examine how the response of the vegetation and the transpiration to drought changes for different vegetation types.

3. Results

The model simulations of total water storage changes are validated against the changes as measured by two GRACE datasets in Fig. 2 to ensure that the simulations adequately represent the observed water balance. The time series of the spatially averaged and deseasonalized (by removing the monthly mean annual cycle) total column water (the sum of the aquifer, soil column, canopy, and snow storages) are shown in Fig. 2a for GW, NGW, and the GRACE4 and GRACE5 observations. Although GRACE5 has been shown to be more accurate than GRACE4, both time series are included in Fig. 2a since GRACE4 extends back to 2002 and gives an indication as to the accuracy of satellite observed changes in terrestrial water storage. The model simulations agree reasonably well with the observations, with a correlation of 0.80 between GRACE5 and GW and 0.71 between GRACE5 and NGW. However, NGW has a higher correlation with GRACE4 than does GW, indicating that the small differences in correlation between GW and NGW may not be important. Both the GW and the NGW simulations reproduce the changes in total column water, although the GW simulation is able to reproduce the magnitude of the water storage anomalies with values approximately 4 kg m^{-2} at the start of 2006, in better agreement than NGW with the 6 kg m^{-2} anomaly seen in GRACE5 during the same period. Time series for GW, NGW, GRACE4, and GRACE5 show a large decline in total water storage corresponding to the 2006 drought (Fig. 2a); however, the decline is smaller for NGW than for GRACE4, GRACE5, and GW. In contrast to NGW, the anomaly in Fig. 2a is positive for the period 2004–06 and primarily negative for the period 2007–09 for both of the observations and GW. For NGW, the water storage changes less over the simulated period and recovers to larger values than GW or the observed changes after the 2006 drought. To understand the reasons behind the differences in GW and NGW in Fig. 2a, the area averaged total water storages changes are decomposed into the contributions from the aquifer and the soil column for the model simulations in Fig. 2b. The variations in soil water from GW and NGW in Fig. 2b are similar in magnitude and timing, although GW is wetter than NGW from 2003 to 2005 (prior to the 2006 drought) and drier from 2007 to 2009. The aquifer in the GW simulations shows a strong drying trend over the simulation period that is not seen in NGW because of the aquifer in NGW being decoupled from the soil column. The decreasing groundwater storage from GW accounts for approximately 30% of the total water storage lost during 2006 and is the reason that GW exhibits a larger decrease in total water storage than NGW in Fig. 2a. The decline in groundwater from the GW simulation qualitatively agree with previous work that demonstrated a decrease in groundwater storage in SE Australia over the period 2001–07 (Leblanc et al. 2009), further validating the accuracy of the simulations. The high correlation between GRACE5 and GW (Fig. 2c) and between GRACE5 and NGW (Fig. 2d) quantitatively demonstrates reasonable agreement between the simulations and the observations. Given that previous work has shown the seasonal cycle in GRACE estimated

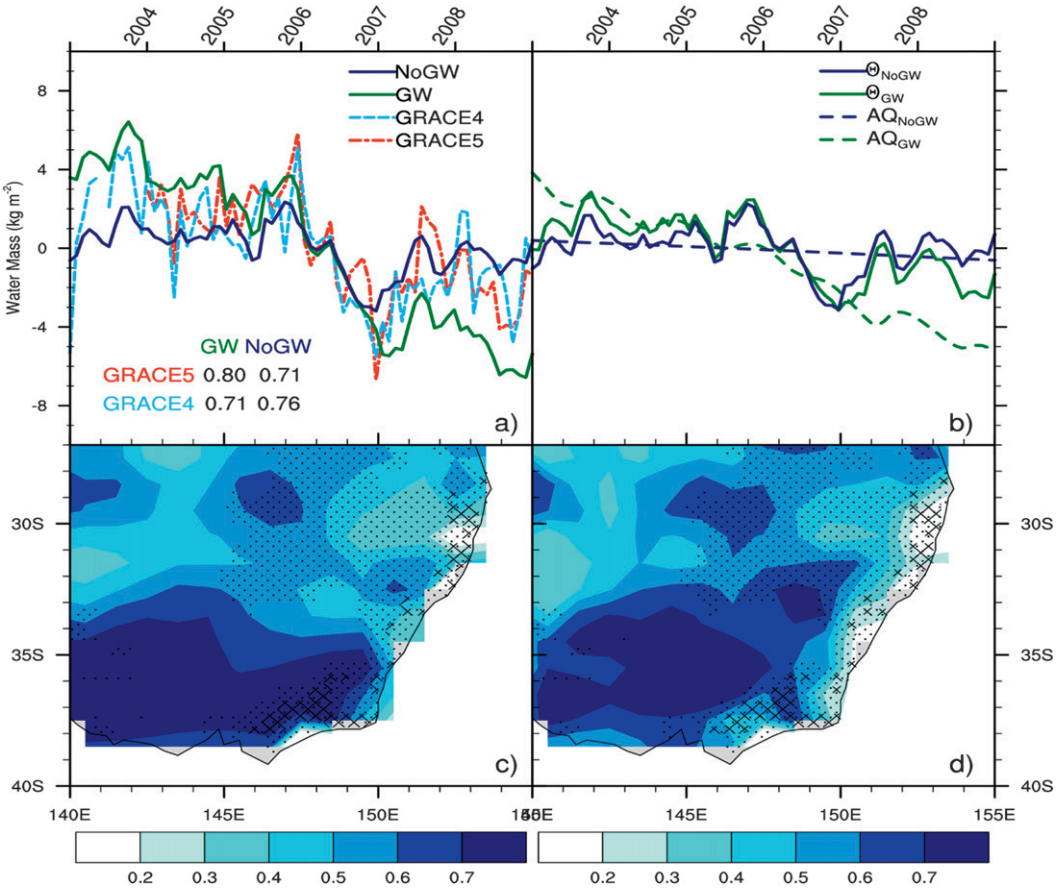

FIG. 2. (a) The spatially averaged (over SE Australia, defined here as 27°–40°S and 140°–155°E) deseasonalized (defined by subtracting the mean annual cycle; in kg m^{-2}) total column water (found as the sum of each soil layer, the aquifer, and the canopy water) from the period 2003–09 for both GRACE datasets (GRACE5 and GRACE4), the GW simulation, and the NGW simulation. The inset table shows the correlation between the spatially averaged GW or the NGW time series and the GRACE5 or GRACE4 data. (b) The deseasonalized water from the same region as (a) broken down into the contributions from the soil column (Θ_{GW} and Θ_{NGW}) and the contribution from the aquifer (AQ_{GW} and AQ_{NGW}) for the GW and the NGW simulations, respectively (in kg m^{-2}). (c) The correlation between GRACE5 and the GW simulation and (d) the correlation between GRACE5 and the NGW simulation over the same time period. The stippling in (b) and (c) shows grid cells covered by at least 60% grass, while the hatching denotes grid cells with at least 85% forest cover.

total water storage changes to have a correlation of 0.83 with observations in Illinois (Yeh et al. 2006), the accuracy of the current simulations are deemed satisfactory. The pattern of correlation is similar between GW and NGW; however, it is clear that GW shows much higher correlations over the grid cells dominated by forests. The GW simulations better capture the changes in spatially averaged total column moisture for the period 2004–09; the NGW simulation has a larger region of correlations greater than 0.6. Overall, the relative performance between the GW and the NGW simulations is difficult to assess from Fig. 2, given both simulations show agreement with the large-scale changes in total column soil moisture.

The suitability of using deseasonalized satellite greenness observations as a proxy for evaluating simulated transpiration (or photosynthesis) is demonstrated in Figs. 3 and 4. The relationship between the deseasonalized monthly photosynthesis (Figs. 3a,b) or transpiration (Figs. 3c,d) and the observed PVF is shown in Fig. 3 for all grid cells in SE Australia with at least 60% coverage by grass (as defined by the default MODIS-derived CLM4 land surface plant function type dataset). Figure 4 shows the relationship between photosynthesis (Figs. 4a,b) or transpiration (Figs. 4c,d) and LAI over the same grassland regions as Fig. 3. Grid cells dominated by grasses are shown in Figs. 3 and 4, as these regions contain shallowly rooted plants that respond

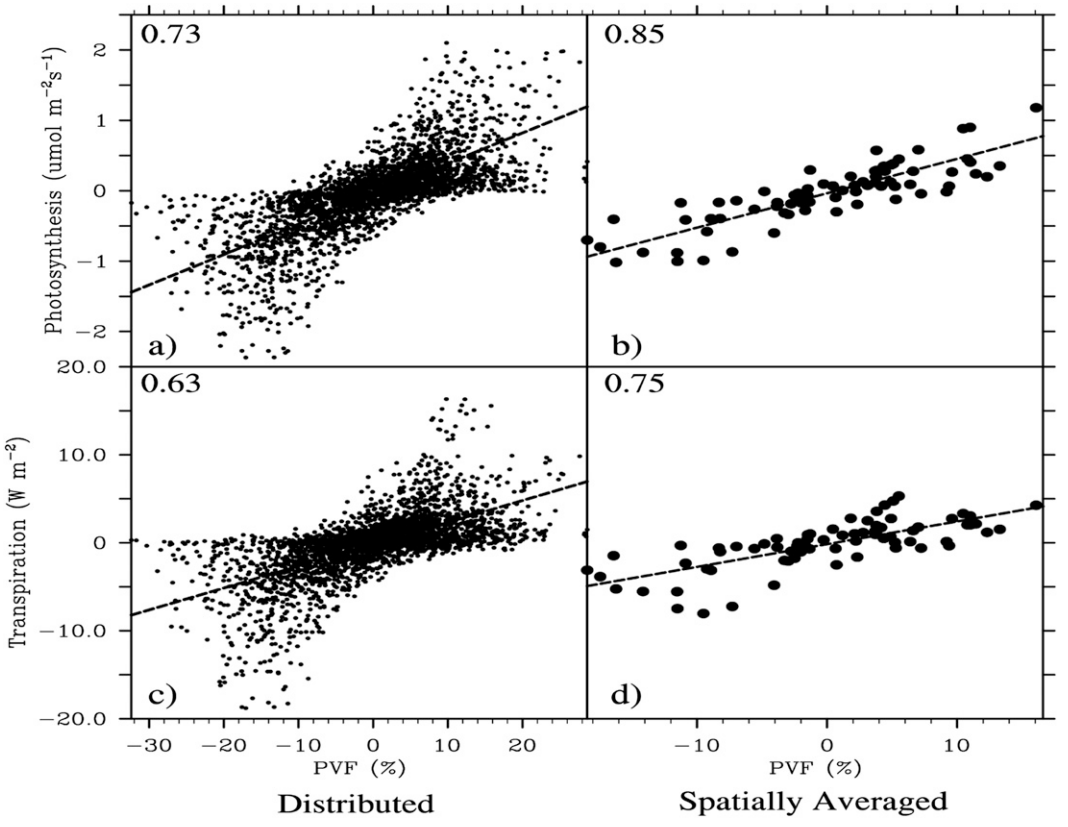

FIG. 3. The deseasonalized (by subtracting the mean annual cycle) monthly (a),(b) photosynthesis and (c),(d) transpiration simulated with CLM4 (GW) as a function of PVF (%) for regions in SE Australia covered with at least 60% grass for the period 2002–08. The individual grid cells are shown in (a) and (c), while (b) and (d) are spatially averaged over all grid cells covered with grass. Also shown are the regression lines and the correlation coefficients between the simulated transpiration or photosynthesis and PVF (upper left corner in each panel).

strongly to interannual rainfall anomalies (see Fig. 5). While there is no physical a priori reason why a linear relationship should exist between transpiration and PVF or LAI, linear regression lines are added to Figs. 3 and 4 to explore the relationship between the simulated and observed variables and to test if the slopes are statistically different from zero.

Figures 3 and 4 show that both vegetation observation types (PVF and LAI) have a distinct and statistically significant relationship (the slope is >0 at the 95% confidence level) for both transpiration and photosynthesis. Comparing Fig. 3c with Fig. 4c (or Fig. 3d with Fig. 4d), it is clear that both photosynthesis and transpiration are related in similar ways to PVF and LAI, even though photosynthesis is more directly related to vegetation greenness. The scatter in the relation between either transpiration or photosynthesis and the vegetation metrics is reduced when the data are averaged spatially over the regions covered predominately by grasslands (Figs. 3b,d as compared to Figs. 3a,c). Spatially averaging reduces the uncertainties associated with using greenness as a transpiration proxy, similar to the regional approach by Chen and Coughenour (2004). The overall positive relationship shown in Figs. 3 and 4 is independent of the vegetation cover, with forests, grasses, and shrubs all showing best fit slopes statistically greater than zero (not shown). Regardless of the many factors that can alter how transpiration relates to vegetation greenness, Figs. 3 and 4 demonstrate that positive transpiration (or photosynthesis) anomalies from the simulations are associated with positive values of vegetation greenness, in agreement with previous work linking NDVI and evapotranspiration (Szilagyi et al. 1998). Therefore, the simulated transpiration (or photosynthesis) should exhibit large temporal variations in the same regions (and over the same plant functional types) that the satellite metrics also exhibit large interannual variations. By comparing how the magnitude and timing of the variations in LAI and PVF change across differing vegetation types with simulated changes in transpiration across the same vegetation types, we

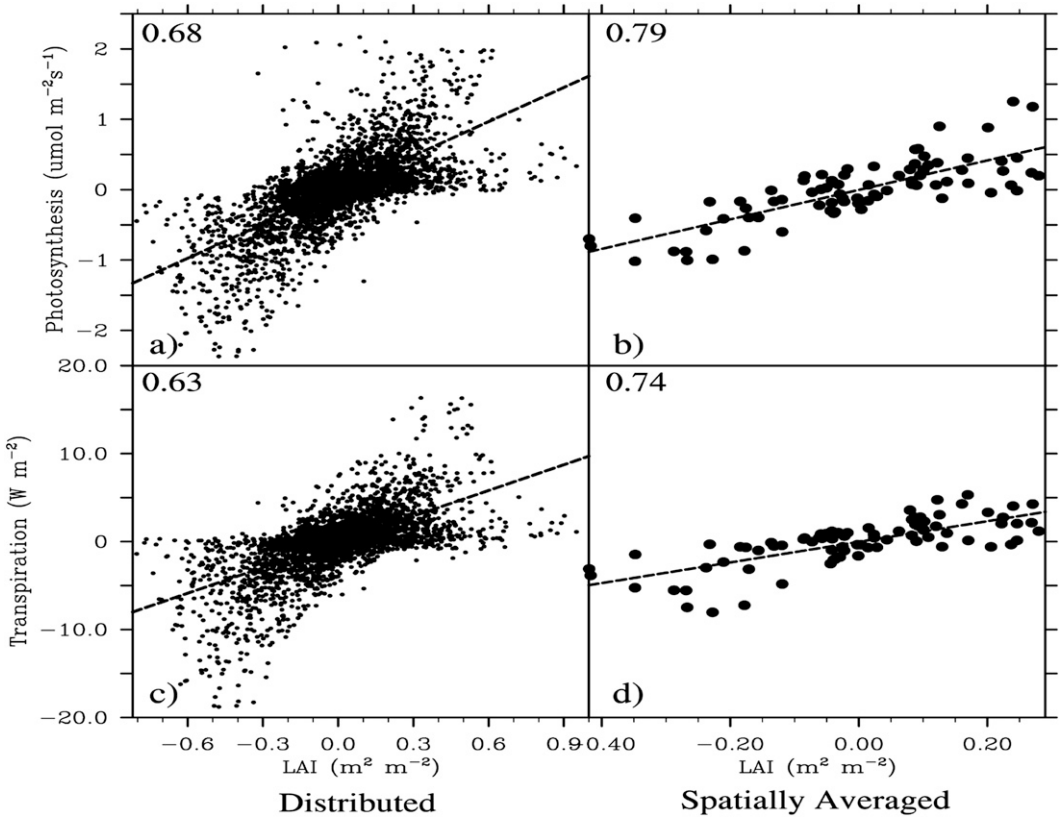

FIG. 4. As in Fig. 3, but as a function of LAI (m^2 m^{-2}).

gain insight into the physically reasonable pattern of transpiration variability.

The variation in scaled (achieved by dividing the time series of anomalies by the temporal mean) transpiration averaged over forested regions of SE Australia is shown in Fig. 5a with the corresponding transpiration over grassland areas shown in Fig. 5b. Simulations with CLM4 coupled with groundwater (simulation GW) can be compared with simulations decoupled from groundwater (NGW) for both vegetation types. Over the forests (Fig. 5a), the NGW transpiration closely matches the rainfall forcing with high interannual variations and a correlation of 0.59. In contrast, in the GW simulation, the interannual anomalies in transpiration are significantly damped and close in magnitude to the observed LAI and PVF (Fig. 5a). The GW simulation, PVF, and LAI are all much less correlated with the precipitation, with values of 0.43, 0.21, and −0.16, respectively. The low correlation for PVF and LAI (and, to a lesser degree, GW) is partially due to the lag between them and the precipitation anomalies (discussed later). Over the grasslands (Fig. 5b), both the NGW and GW simulations and the observed vegetation metrics show larger interannual variability than over forested areas, and all four quantities are well correlated with the precipitation. The anomalies are again damped in the GW simulations as compared to NGW (although not to the same degree as over forests) and closely match the observed variations in the vegetation. Most significantly, the transpiration flux in the NGW simulation shows a large decline over the forests associated with the 2003 and the 2006 droughts (Fig. 5a), a decline that does not occur in the GW simulation and is not implied in the vegetation greenness observations. This is apparent, to a lesser degree, over the grasslands.

The relationship between rainfall and transpiration anomalies is shown for all forest points in Fig. 6a and all grassland points in Fig. 6b. The regression lines show a near one-to-one correspondence between rainfall and transpiration in the NGW simulations over forests and grasslands, with correlations of 0.59 and 0.68, respectively. In contrast, the scaled variations in the GW simulation over forests highlight a very strong suppression of rainfall-driven variability in transpiration. For the GW simulations, the slope of the best fit line is statistically larger (at the 95% confidence level) over grasses than forests, while the slopes from the NGW simulations are statistically indistinguishable at the 95% confidence

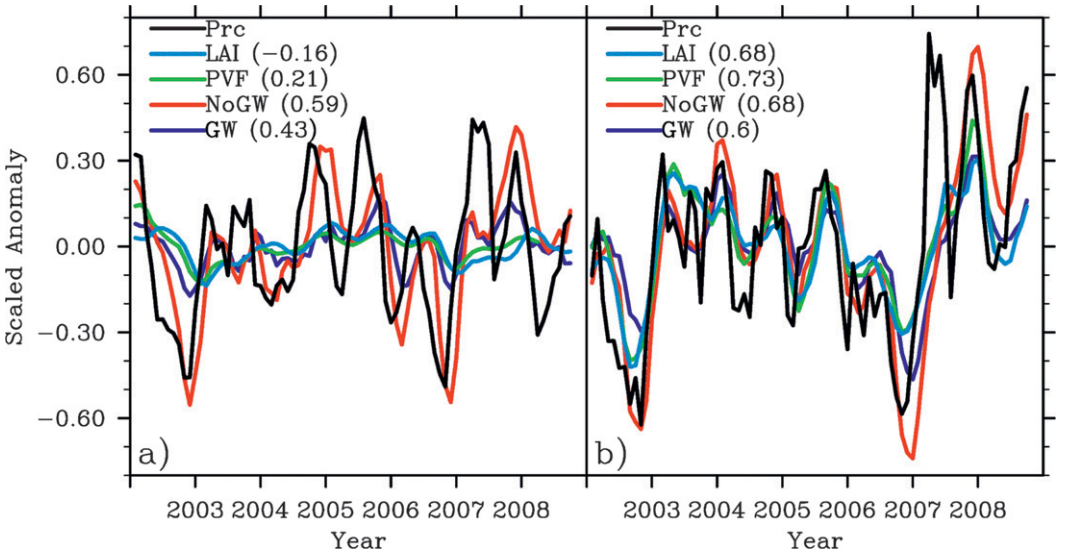

FIG. 5. The scaled (performed by dividing by the temporal mean), deseasonalized (the mean annual cycle is removed), and smoothed (with a 3-month moving average) LAI, PVF, transpiration for the GW and the NGW simulations, and precipitation spatially averaged over grid cells with (a) >85% forest cover and (b) >60% grasses. The correlation between each of the time series and the precipitation is shown in parentheses.

level. These anomalies are larger in the GW simulations over grasslands but are still significantly lower than in the NGW simulations as the GW slope is smaller than the NGW slope at the 95% confidence level.

The probability density function (PDF) of the standard deviation of the scaled and deseasonalized transpiration, LAI, PVF, and precipitation (Fig. 6c for all forest grid points and Fig. 6d for grasslands) highlights the limited variability in the transpiration flux for the GW simulations as opposed to the NGW simulations. The LAI, PVF, and the GW simulations show little interannual variations over the forests, with the distribution peaking near zero, while the precipitation and NGW simulations show much greater variability. The NGW simulations closely match the variability in precipitation regardless of the vegetation cover, while PVF, LAI, and the GW simulations show lower variability than the precipitation, especially over forested regions.

The extent to which interannual transpiration anomalies are delayed relative to the precipitation anomalies due to groundwater in forested regions in SE Australia are illustrated in Fig. 7. Figure 7 shows the lag (in months) that results in the maximum correlation between the simulated interannual transpiration for the GW simulation (Fig. 7a), the NGW simulation (Fig. 7b), and the observations (Figs. 7c,d). The GW simulation, PVF, and LAI are maximally correlated with the precipitation anomalies at a lag of 4–9 months in the forested regions (hatched), while the grasslands and shrubs are maximally correlated at a lag of 0–1 months. In contrast, the NGW simulations correlate most strongly with a lag of 0–1 months everywhere, independent of the vegetation cover. Similar to the magnitude of the transpiration anomalies, the observations and the GW runs show a clear difference in the timing of the land surface response to drought depending on the land cover type. The NGW simulations fail to exhibit this behavior because the transpiration anomalies are more closely related to the precipitation anomalies (Figs. 5a,b and 6c,d).

Finally, Fig. 8 shows the difference in the standard deviation of the soil moisture contained in the 10 soil layers and also indicates areas with >85% forest cover (hatched). The soil moisture variability increases in the NGW simulation relative to the GW simulation, mainly in areas coincident with the forests. The increased soil moisture variability in the NGW simulations seen in Fig. 8 drives the larger transpiration anomalies seen in Figs. 5 and 6.

4. Discussion

The simulations using CLM4 with groundwater (GW) substantially decouple the simulated transpiration from the precipitation forcing over the forests of SE Australia. If groundwater is included, significant rainfall variability, shown in Fig. 1a, does not drive large variability in transpiration in forest regions. Specifically, a precipitation anomaly change from +0.5 to −0.4 only reduces transpiration by 30% (from +0.15

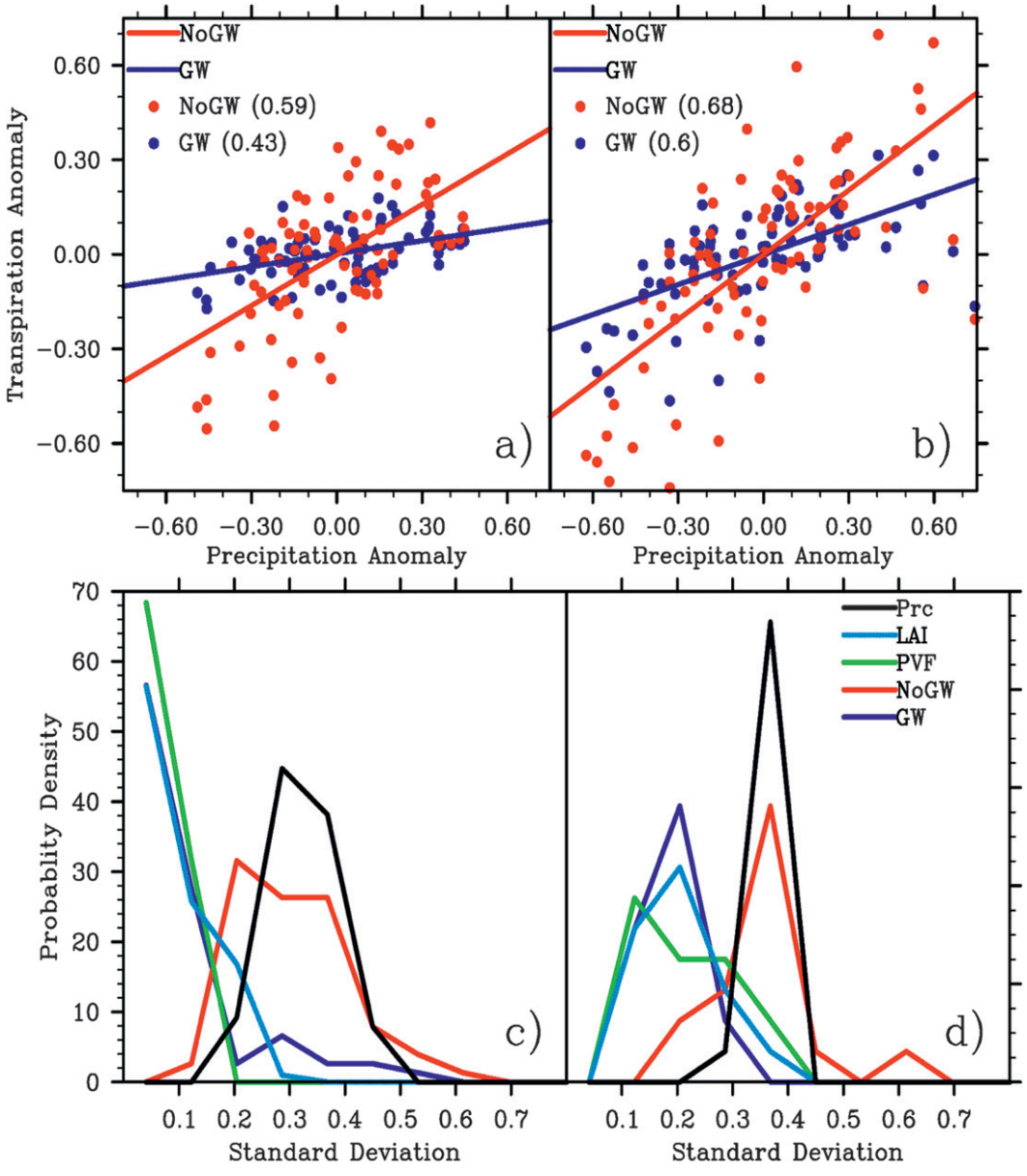

FIG. 6. Scatterplots of the spatially averaged, scaled (by dividing by the mean), and deseasonalized (by removing the mean annual cycle) transpiration from the GW (blue) and NGW (red) runs plotted and regressed against precipitation from (a) the same forested regions and (b) the same grassland areas as Figs. 5a and 5b, respectively. The line of best fit and the correlation (in parenthesis) are also shown. PDFs of the distributed standard deviation (at each grid cell) of the deseasonalized and scaled PVF (green), LAI (cyan), GW transpiration (blue), NGW transpiration (red), and precipitation (black) over the same (c) forested and (d) grassland areas.

to −0.15). This is in agreement with the observed variation in LAI and PVF, which suggests that the groundwater-coupled simulations are likely more realistic than the NGW simulations where the same precipitation anomaly reduces transpiration by 95% (from +0.2 to −0.75). The low variability in the GW simulation is caused by a reduction in the soil moisture variability due to groundwater maintaining a wetter soil profile, as on average GW has approximately 400 kg m^{-2} more total soil moisture than NGW in the forested regions, resulting in a reduction of transpiration variability. A careful analysis of Fig. 5a shows periods of lower rainfall do lead to a reduction in transpiration and observed vegetation greenness as one would expect, but the scale of the decline is negligible compared to simulations where groundwater is excluded. In the grassland areas, the

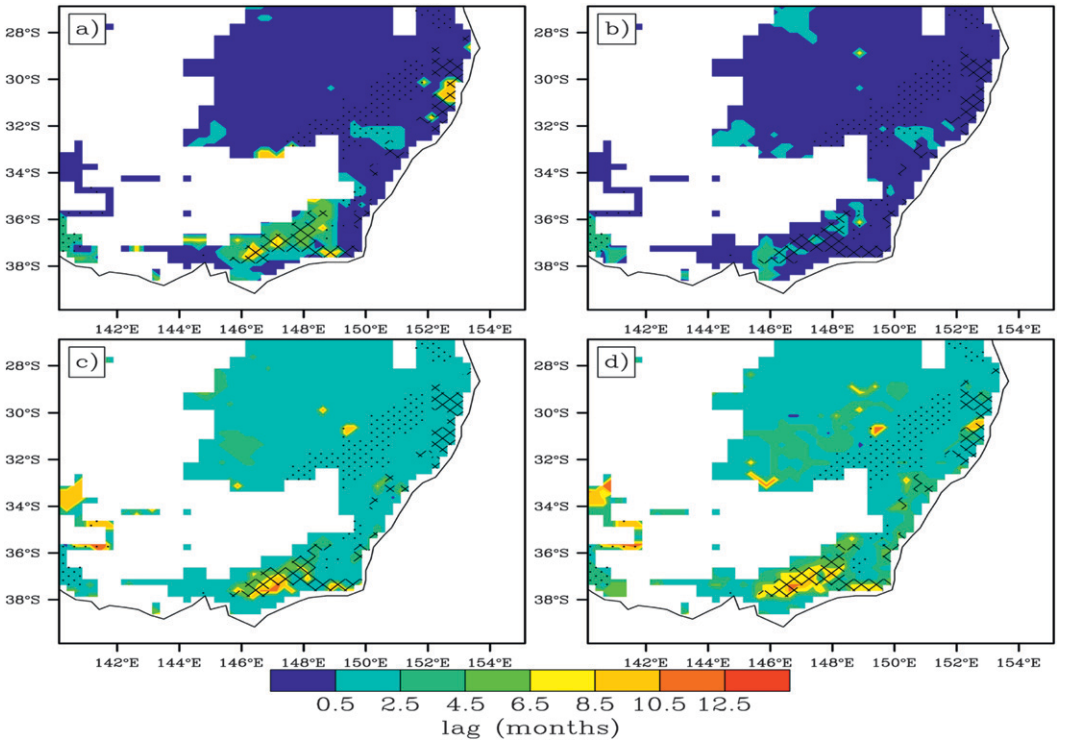

FIG. 7. The lag in months that results in the maximum correlation between the deseasonalized (the mean annual cycle is removed) precipitation (with the precipitation leading) and (a) the simulated transpiration from GW, (b) the simulated transpiration from NGW, (c) PVF, and (d) LAI. Only regions with >60% coverage of natural vegetation are shown so that bare soil and crops are excluded. The stippling indicates regions covered by at least 60% grasses, and the areas with at least 85% forest cover are marked with hatching.

roots of the vegetation cannot tap the lower soil layers as all roots are contained in the top 1 m. However, in the GW simulations, an upward diffusion of moisture into the soil column helps maintain enough soil moisture to suppress some of the extreme variability seen in the NGW simulation (Fig. 5b), a process noted by Pokhrel et al. (2012). Our results therefore suggest that it is not only deeply rooted, forest-based, groundwater-dependent ecosystems that are sensitive to the representation of groundwater.

The suppression of variability in the transpiration simulated by CLM4 in the presence of groundwater has several implications. First, in agreement with the observed variability in LAI and PVF, transpiration and photosynthesis is sustained in the GW simulations (see Fig. 5). While a reduction in precipitation of 90% of the mean in the NGW simulation reduces transpiration by 95% of the mean, the same precipitation reduction only reduces transpiration by 30% in the GW simulation. As a result, the sustained transpiration provides the trees a capacity to maintain growth through dry periods, something that has been shown in tropical regions previously (Fan and Miguez-Macho 2010). This has important implications if leaf area index or the vegetation is simulated dynamically. In the NGW simulations, the suppression of photosynthesis during drought would lead to a reduction in net primary productivity, potential vegetation dieback, and a loss of carbon stored in the landscape. This is a positive feedback that would tend to accentuate drought. In contrast, in the GW simulations, enough photosynthesis is maintained to sustain the vegetation through the drought and reduce any tendency to transition a region from trees to grass. The inclusion of groundwater therefore reduces the likelihood of drought-triggered abrupt changes in terrestrial systems. While we cannot quantify this reduction, the result raises questions about existing assessments of ecosystem vulnerability to climate change (e.g., Lenton et al. 2008) given most simulations to date lack the buffering effect of groundwater.

A second implication of our results relates to the simulation of land use and land cover change (LULCC). Unlike dynamic vegetation experiments where the simulated vegetation responds to an applied forcing, in LULCC experiments the model sensitivity to anthropogenic changes in vegetation (such as deforestation) is evaluated

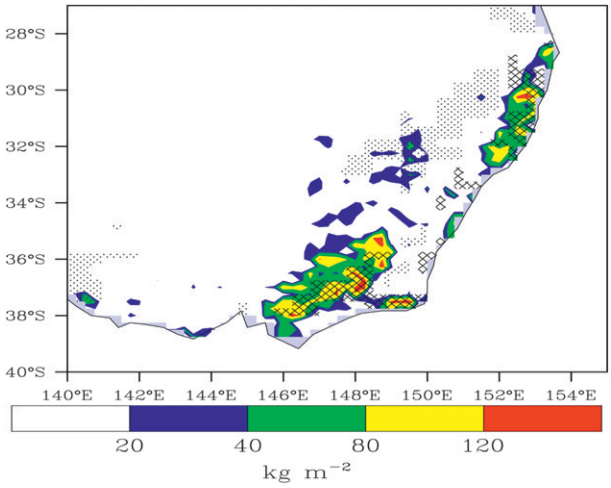

FIG. 8. The difference in the standard deviation of the deseasonalized (by removing the mean annual cycle) total column soil moisture (in kg m^{-2}) between the NGW and GW simulations. The stippling indicates regions covered by at least 60% grasses, and the areas with at least 85% forest cover are marked with hatching.

by specifying changes in land cover types. Pielke et al. (2011) discuss how large-scale transformation of vegetation from forest to grasslands can affect the regional meteorology and climatology. Simulations of LULCC in global and regional climate models generally omit the influence of groundwater, with the exception of Findell et al. (2006) and Molders and Ruhaak (2002). Thus, the change represented in simulations to date (where the forest plant functional types are replaced with grass or crops) is approximated by the NGW simulation for forest (with high variability; Figs. 5a, 6c) to the NGW simulation for grass (with high variability; Figs. 5b, 6d). Our study shows that if groundwater is included, the forest simulations display a damped response to drought, but if it is transformed to grass, and largely decoupled from the groundwater, it displays increased variability. This may not affect the impact of LULCC on the mean regional climate, but it has the potential to affect the impact of LULCC on regional climate extremes (Avila et al. 2012).

Finally, feedbacks between the land surface and the atmosphere affect the simulated climate (Betts et al. 1996; Evans et al. 2011). In our NGW simulations, as the rainfall anomaly intensifies, transpiration declines (Fig. 5). This would necessitate a change in the partitioning of available energy from latent to sensible heat with a tendency to warm and dry the boundary layer. This positive feedback has the potential to exacerbate drought (Hong and Kalnay 2000). In contrast, in our GW simulations, the same rainfall anomaly leads to very small declines in transpiration, such that the latent heat flux can continue to cool and moisten the boundary layer with the potential to slow the onset of drought. Our results therefore suggest that modeling systems that ignore groundwater, used for seasonal prediction, decadal prediction, or climate projection, will tend to overemphasize the response of transpiration to declining rainfall over forested regions with consequential misrepresentation of feedbacks on the boundary layer. The impact of groundwater on transpiration is dependent on the vegetation cover type and the regional meteorology, including the scale of rainfall recycling. Hence, regional modeling studies that contain forested areas similar to those in SE Australia and with a similar regional meteorology are likely to show similar sensitivities.

There are potential implications (dieback, LULCC, and feedbacks) of the importance of groundwater in forested ecosystems beyond SE Australia, of course. The Amazon forest has been shown to be dependent on uptake of water from deep within the soil column (Nepstad et al. 1994), with evidence showing water withdrawal at depths of up to 18 m (Davidson et al. 2011). Some evidence exists from modeling studies over the Amazon (Kleidon and Heimann 2000) that deep roots play an important role in how LULCC affects regional climate. The mitigation of transpiration anomalies shown in Fig. 5 and the reduced soil moisture variations in Fig. 8 from the inclusion of groundwater provide further evidence that deep roots may play a broadly significant role.

The current study has several limitations, in part because of the use of a simple one-dimensional land surface model. CLM4 neglects an explicit representation of the lateral redistribution of soil water, a process that can influence the mean gridcell water content and land surface fluxes (Huang and Leng 2008; Rihani et al. 2010). The subsurface heterogeneity in soils and its impact on latent heat fluxes (Williams and Maxwell 2011) are also neglected in the model. The small-scale spatial heterogeneity of transpiration response to drought seen in observations cannot be captured by the coarse resolution of CLM4 (Eberbach and Burrows 2006). We use the default CLM4 hydrology parameters because previous work has demonstrated the resilience of land surface–groundwater models to parameter changes (Gulden et al. 2007). However, optimization of the hydrological parameters can generate more accurate simulations when suitable observations are available (Li et al. 2011). Finally, the root depth concentration in CLM4 does not make explicit use of any knowledge about eucalypts. Future work will attempt to address these issues by incorporating more complex models of subsurface hydrology and parameters derived specifically for Australian vegetation.

5. Conclusions

We have explored how the inclusion of groundwater within an LSM affects the impact of rainfall variability on transpiration over SE Australia. Between 2002 and 2009, two significant droughts occurred over this region. We have shown that interannual anomalies in the observed vegetation are closely related to the simulated photosynthesis and transpiration, revealing that the satellite vegetation observations provide a tool to diagnose the LSM response to drought. We have shown that if groundwater is included, the impact of these droughts on transpiration variability from the forested regions is very small and is in agreement with the observed vegetation variability. However, if groundwater is omitted, the variability in transpiration from the forests largely reflects rainfall variability. The presence of groundwater in the model, combined with deeply rooted vegetation, allows the forests to withstand the variability in rainfall and sustain transpiration in general agreement with the observed vegetation variability. The groundwater also delays the land surface response to the large precipitation anomalies by several months over forested regions, in agreement with the observed vegetation variability. While the shallow-rooted grasslands display higher variability than the forests in both the GW and NGW simulations, the inclusion of groundwater still reduces variability in transpiration because it helps maintain a wetter soil profile.

Our results indicate that failure to include groundwater in regions like SE Australia, where groundwater sustained ecosystems coupled with very deeply rooted eucalypts are common, has some serious implications. First, the dampening of variability by groundwater means that the forests sustain transpiration and likely reduce the intensity of drought by maintaining a moisture flux into the atmosphere, rather than switching to a sensible heat-dominated surface energy balance with resulting warming and drying of the boundary layer. Second, if vegetation or leaf area index are simulated dynamically, failure to include groundwater will tend to oversimulate variability in transpiration and photosynthesis, leading to a higher likelihood of simulated dieback during droughts. Finally, failure to represent groundwater would lead to a misrepresentation of the impacts of land use and land cover change in regions where forests are sustained by groundwater.

Acknowledgments. All authors acknowledge support from the Australian Research Council Super Science scheme (FS100100054). A.J.P. was also supported by the Australian Research Council Centre of Excellence for Climate System Science (CE110001028). We thank Dr. Peter Smith for his advice on parts of this paper. Finally, the GRACE land data were processed by Sean Swenson, supported by the NASA MEaSUREs Program, and are available at http://grace.jpl.nasa.gov.

REFERENCES

Anyah, R. O., C. P. Weaver, G. Miguez-Macho, Y. Fan, and A. Robock, 2007: Incorporating water table dynamics in climate modeling: 3. Simulated groundwater influence on coupled land–atmosphere variability. *J. Geophys. Res.,* **113,** D07103, doi:10.1029/2007JD009087.

Avila, F., A. J. Pitman, M. Donat, L. Alexander, and G. Abramowitz, 2012: Climate model simulated changes in temperature extremes due to land cover change. *J. Geophys. Res.,* **117,** D04108, doi:10.1029/2011JD016382.

Benyon, R. G., S. Theiveyanathan, and T. M. Doody, 2006: Impacts of tree plantations on groundwater in south-eastern Australia. *Aust. J. Bot.,* **54,** 181–192.

Berg, A. A., J. S. Famiglietti, J. P. Walker, and P. R. Houser, 2003: Impact of bias correction to reanalysis products on simulations of North American soil moisture and hydrological fluxes. *J. Geophys. Res.,* **108,** 4490, doi:10.1029/2002JD003334.

Betts, A. K., J. H. Ball, A. C. M. Beljaars, M. J. Miller, and P. A. Viterbo, 1996: The land surface-atmosphere interaction: A review based on observational and global modeling perspectives. *J. Geophys. Res.,* **101,** 7209–7225.

Buermann, W., Y. Wang, J. Dong, L. Zhou, X. Zeng, R. E. Dickinson, C. S. Potter, and R. B. Myneni, 2002: Analysis of a multiyear global vegetation leaf area index data set. *J. Geophys. Res.,* **107,** 4646, doi:10.1029/2001JD000975.

Cai, W., T. Cowan, P. Briggs, and M. Raupach, 2009: Rising temperature depletes soil moisture and exacerbates severe drought conditions across southeast Australia. *Geophys. Res. Lett.,* **36,** L21709, doi:10.1029/2009GL040334.

Canadell, J., R. B. Jackson, J. R. Ehleringer, H. A. Mooney, O. E. Sala, and E.-D. Schulze, 1996: Maximum rooting depth of vegetation types at the global scale. *Oecologia,* **108,** 583–595.

Chen, D.-X., and M. B. Coughenour, 2004: Photosynthesis, transpiration, and primary productivity: Scaling up from leaves to canopies and regions using process models and remotely sensed data. *Global Biogeochem. Cycles,* **18,** GB4033, doi:10.1029/2002GB001979.

Cowan, I. R., 1982: Regulation of water use in relation to carbon gain in higher plants. *Encyclopedia of Plant Physiology,* O. L. Lange et al., Eds., Springer-Verlag, 589–614.

Cowling, S. A., and C. B. Field, 2003: Environmental controls of leaf area production: Implications for vegetation and land surface modeling. *Global Biogeochem. Cycles,* **17,** 1007, doi:10.1029/2002GB001915.

Davidson, E., and Coauthors, 2011: Carbon inputs and water uptake in deep soils of an eastern Amazon forest. *For. Sci.,* **57,** 51–58.

Decker, M., and X. Zeng, 2009: Impact of the modified Richards equation on global soil moisture simulation in the Community Land Model (CLM3.5). *J. Adv. Model. Earth Syst.,* **1,** 22 pp. [Available online at http://james.agu.org/index.php/JAMES/article/viewArticle/v1n5.]

——, M. A. Brunke, Z. Wang, K. Sakaguchi, X. Zeng, and M. Bosilovich, 2012: Evaluation of the reanalysis products

from GSFC, NCEP, and ECMWF using flux tower observations. *J. Climate,* **25,** 1916–1944.

Eamus, D., and R. Froend, 2006: Groundwater-dependent ecosystems: The where, what and why of GDEs. *Aust. J. Bot.,* **54,** 91–96.

Eberbach, P. L., and G. E. Burrows, 2006: The transpiration response by four topographically distributed *Eucalyptus* species, to rainfall occurring during drought in south eastern Australia. *Physiol. Plant.,* **127,** 483–493.

Evans, J. P., A. J. Pitman, and F. T. Cruz, 2011: Coupled atmospheric and land surface dynamics over southeast Australia: A review, analysis and identification of future research priorities. *Int. J. Climatol.,* **31,** 1758–1772.

Fan, Y., and G. Miguez-Macho, 2010: Potential groundwater contribution to Amazon dry-season evapotranspiration. *Hydrol. Earth Syst. Sci.,* **14,** 2039–2056.

——, ——, C. P. Weaver, R. Walko, and A. Robock, 2007: Incorporating water table dynamics in climate modeling: 1. Water table observations and the equilibrium water table simulations. *J. Geophys. Res.,* **112,** D10125, doi:10.1029/2006JD008111.

Findell, K. L., T. R. Knutson, and P. C. D. Milly, 2006: Weak simulated extratropical responses to complete tropical deforestation. *J. Climate,* **19,** 2835–2850.

Gent, P. R., and Coauthors, 2011: The Community Climate System Model version 4. *J. Climate,* **24,** 4973–4991.

Gotangco Castillo, C. K., S. Levis, and P. Thornton, 2012: Evaluation of the new CNDV option of the Community Land Model: Effects of dynamic vegetation and interactive nitrogen on CLM4 means and variability. *J. Climate,* **25,** 3702–3714.

Guerschman, J. P., M. J. Hill, L. J. Renzullo, D. J. Barrett, A. S. Marks, and E. J. Botha, 2009: Estimating fractional cover of photosynthetic vegetation, non-photosynthetic vegetation and bare soil in Australian tropical savanna region upscaling the EO-1 Hyperion and MODIS sensors. *Remote Sens. Environ.,* **113,** 928–945.

Gulden, L. E., E. Rosero, Z.-L. Yang, M. Rodell, C. S. Jackson, G.-Y. Niu, J.-F. P. Yeh, and J. Famiglietti, 2007: Improving land-surface model hydrology: Is an explicit aquifer model better than a deeper soil profile? *Geophys. Res. Lett.,* **34,** L09402, doi:10.1029/2007GL029804.

Hong, S.-Y., and E. Kalnay, 2000: Role of sea surface temperature and soil-moisture feedback in the 1998 Oklahoma-Texas drought. *Nature,* **408,** 842–844.

Huang, M. X. L., and L. R. Leng, 2008: A generalized subsurface flow parameterization considering subgrid spatial variability of recharge and topography. *J. Hydrometeor.,* **9,** 1151–1171.

Jackson, R. B., J. Canadell, J. R. Ehleringer, H. A. Mooney, O. E. Sala, and E. D. Schulze, 1996: A global analysis of root distributions for terrestrial biomes. *Oecologia,* **108,** 389–411.

Jones, D. A., W. Wang, and R. Fawcett, 2009: High-quality spatial climate data-sets for Australia. *Aust. Meteor. Oceanogr. J.,* **58,** 233–248.

Kleidon, A., and M. Heimann, 2000: Assessing the role of deep rooted vegetation in the climate system with model simulations: Mechanism, comparison to observations and implications for Amazonian deforestation. *Climate Dyn.,* **16,** 183–199.

Kollet, S. J., and R. M. Maxwell, 2008: Capturing the influence of groundwater dynamics on land surface processes using an integrated, distributed watershed model. *Water Resour. Res.,* **44,** W02402, doi:10.1029/2007WR006004.

Landerer, F. W., and S. C. Swenson, 2012: Accuracy of scaled GRACE terrestrial water storage estimates. *Water Resour. Res.,* **48,** W04531, doi:10.1029/2011WR011453.

Landsberg, J. J., and F. J. Hingston, 1996: Evaluating a simple radiation dry matter conversion model using data from *Eucalyptus globulus* plantations in Western Australia. *Tree Physiol.,* **16,** 801–808.

Lawrence, D. M., K. W. Oleson, M. G. Flanner, C. G. Fletcher, P. J. Lawrence, S. Levis, S. C. Swenson, and G. B. Bonan, 2012: The CCSM4 land simulation, 1850– 2005: Assessment of surface climate and new capabilities. *J. Climate,* **25,** 2240–2260.

Leblanc, M. J., P. Tregoning, G. Ramillien, S. O. Tweed, and A. Fakes, 2009: Basin-scale, integrated observations of the early 21st century multiyear drought in southeast Australia. *Water Resour. Res.,* **45,** W04408, doi:10.1029/2008WR007333.

Lenton, T. M., H. Held, E. Kriegler, J. W. Hall, W. Lucht, S. Rahmstorf, and H. J. Schellnhuber, 2008: Tipping elements in the Earth's climate system. *Proc. Natl. Acad. Sci. USA,* **105,** 1786–1793, doi:10.1073/pnas.0705414105.

Leung, L. R., M. Huang, Y. Qian, and X. Liang, 2011: Climate–soil–vegetation control on groundwater table dynamics and its feedbacks in a climate model. *Climate Dyn.,* **36,** 57–81.

Li, H., M. Huang, M. S. Wigmosta, Y. Ke, A. M. Coleman, L. R. Leung, A. Wang, and D. M. Ricciuto, 2011: Evaluating runoff simulations from the Community Land Model 4.0 using observations from flux towers and a mountainous watershed. *J. Geophys. Res.,* **116,** D24120, doi:10.1029/2011JD016276.

Liang, X., Z. Xie, and M. Huang, 2003: A new parameterization for surface and groundwater interactions and its impact on water budgets with the variable infiltration capacity (VIC) land surface model. *J. Geophys. Res.,* **108,** 8613, doi:10.1029/2002JD003090.

Lo, M.-H., P. J.-F. Yeh, and J. S. Famigletti, 2008: Constraining water table depth simulations in a land surface model using estimated baseflow. *Adv. Water Resour.,* **31,** 1552–1564.

——, J. S. Famigletti, P. J.-F. Yeh, and T. H. Syed, 2010: Improving parameter estimation and water table depth simulation in a land surface model using GRACE water storage and estimated baseflow data. *Water Resour. Res.,* **46,** W05517, doi:10.1029/2009WR007855.

Maxwell, R. M., F. K. Chow, and S. J. Kollet, 2007: The groundwater–land-surface–atmosphere connection: Soil moisture effects on the atmospheric boundary layer in fully-coupled simulations. *Adv. Water Resour.,* **30,** 2447–2466.

——, J. K. Lundquist, J. D. Mirocha, S. G. Smith, C. S. Woodward, and A. F. B. Tompson, 2011: Development of a coupled groundwater–atmospheric model. *Mon. Wea. Rev.,* **139,** 96–116.

McMurtrie, R. E., R. Leuning, W. A. Thompson, and A. M. Wheeler, 1992: A model of canopy photosynthesis and water use incorporating a mechanistic formulation of leaf CO_2 exchange. *For. Ecol. Manage.,* **52,** 261–278.

Miguez-Macho, G., Y. Fan, C. P. Waever, R. Walko, and A. Robock, 2007: Incorporating water table dynamics in climate modeling. 2: Formulation, validation, and soil moisture simulation. *J. Geophys. Res.,* **112,** D13108, doi:10.1029/2006JD008112.

Molders, N., and W. Ruhaak, 2002: On the impact of explicitly predicted runoff on the simulated atmospheric response to small-scale land-use change—An integrated modeling approach. *Atmos. Res.,* **63,** 3–38.

Mu, Q., F. A. Heinsch, M. Zhao, and S. W. Running, 2007: Development of a global evapotranspiration algorithm based on

MODIS and global meteorology data. *Remote Sens. Environ.*, **111,** 519–536.

Nepstad, D. C., and Coauthors, 1994: The role of deep roots in the hydrological and carbon cycles of Amazonian forests and pastures. *Nature,* **372,** 666–669.

Ngo-Duc, T., K. Laval, G. Ramillien, J. Polcher, and A. Cazenave, 2007: Validation of the land water storage simulated by Organising Carbon and Hydrology in Dynamic Ecosystems (ORCHIDEE) with Gravity Recovery and Climate Experiment (GRACE) data. *Water Resour. Res.,* **43,** W04427, doi:10.1029/2006WR004941.

Niu, G.-Y., Z.-L. Yang, R. E. Dickinson, L. E. Gulden, and H. Su, 2007: Development of a simple groundwater model for use in climate models and evaluation with Gravity Recovery and Climate Experiment data. *J. Geophys. Res.,* **112,** D07103, doi:10.1029/2006JD007522.

O'Grady, A. P., D. Eamus, and L. B. Hutley, 1999: Transpiration increases during the dry season: Patterns of tree water use in eucalypt open-forests of northern Australia. *Tree Physiol.,* **19,** 591–597.

——, ——, P. G. Cook, and S. Lamontagne, 2006: Groundwater use by riparian vegetation in the wet–dry tropics of northern Australia. *Aust. J. Bot.,* **54,** 145–154, doi:10.1071/BT04164.

Oleson, K. W., and Coauthors, 2008: Improvements to the Community Land Model and their impact on the hydrological cycle. *J. Geophys. Res.,* **113,** G01021, doi:10.1029/2007JG000563.

——, and Coauthors, 2010: Technical description of version 4.0 of the Community Land Model (CLM). NCAR Tech. Note NCAR/TN-478+STR, National Center for Atmospheric Research, Boulder, CO, 257 pp.

Pan, M., and Coauthors, 2003: Snow process modeling in the North American Land Data Assimilation System (NLDAS): 2. Evaluation of model simulated snow water equivalent. *J. Geophys. Res.,* **108,** 8850, doi:10.1029/2003JD003994.

Pielke, R. A., Sr., and Coauthors, 2011: Land use/land cover changes and climate: Modeling analysis and observational evidence. *Wiley Interdiscip. Rev.: Climatic Change,* **2,** 828–850, doi:10.1002/wcc.144.

Pokhrel, Y., N. Hanasaki, S. Koirala, J. Cho, P. J.-F. Yeh, H. Kim, S. Kanae, and T. Oki, 2012: Incorporating anthropogenic water regulation modules into a land surface model. *J. Hydrometeor.,* **13,** 255–269.

Qian, T., A. Dai, K. E. Trenberth, and K. W. Oleson, 2006: Simulation of global land surface conditions from 1948–2004. Part I: Forcing data and evaluation. *J. Hydrometeor.,* **7,** 953–975.

Reichle, R. H., R. D. Koster, G. J. M. De Lannoy, B. A. Forman, Q. Liu, S. P. P. Mahanama, and A. Touré, 2011: Assessment and enhancement of MERRA land surface hydrology estimates. *J. Climate,* **24,** 6322–6338.

Rice, K. J., S. L. Matzner, W. Byer, and J. R. Brown, 2004: Patterns of tree dieback in Queensland, Australia: The importance of drought stress and the role of resistance to cavitation. *Oecologia,* **139,** 190–198.

Rienecker, M., and Coauthors, 2011: MERRA: NASA's Modern-Era Retrospective Analysis for Research and Applications. *J. Climate,* **24,** 3624–3648.

Rihani, J., R. M. Maxwell, and F. K. Chow, 2010: Coupling groundwater and land-surface processes: Idealized simulations to identify effects of terrain and subsurface heterogeneity on land surface energy fluxes. *Water Resour. Res.,* **46,** W12523, doi:10.1029/2010WR009111.

Robock, A., and Coauthors, 2003: Evaluation of the North American Land Data Assimilation System over the southern Great Plains during the warm season. *J. Geophys. Res.,* **108,** 8846, doi:10.1029/2002JD003245.

Rosero, E., Z. L. Yang, L. E. Gulden, G. Y. Niu, and D. J. Gochis, 2009: Evaluating enhanced hydrological representations in Noah LSM over transition zones: Implications for model development. *J. Hydrometeor.,* **10,** 600–622.

Sacks, W. J., B. I. Cook, N. Buenning, S. Levis, and J. H. Helkowski, 2009: Effects of global irrigation on the near-surface climate. *Climate Dyn.,* **33,** 159–175, doi:10.1007/s00382-008-0445-z.

Sakaguchi, K., X. Zeng, B. J. Christoffersen, N. Restrepo-Coupe, S. R. Saleska, and P. M. Brando, 2011: Natural and drought scenarios in an east central Amazon forest: Fidelity of the Community Land Model 3.5 with three biogeochemical models. *J. Geophys. Res.,* **116,** G01029, doi:10.1029/2010JG001477.

Schenk, H. J., and R. B. Jackson, 2002: The global biogeography of roots. *Ecol. Monogr.,* **72,** 311–328.

Seuffert, G., P. Gross, and C. Simmer, 2002: The influence of hydrologic modeling on the predicted local weather: Two-way coupling of a mesoscale weather prediction model and a land surface hydrologic model. *J. Hydrometeor.,* **3,** 505–523.

Sinclair, T. R., and T. Horie, 1989: Leaf nitrogen, photosynthesis, and crop radiation use efficiency: A review. *Crop Sci.,* **29,** 90–98.

Stöckli, R., and Coauthors, 2008: The use of Fluxnet in the Community Land Model development. *J. Geophys. Res.,* **113,** G01025, doi:10.1029/2007JG000562.

Szilagyi, J., D. C. Rundquist, and D. C. Gosseli, 1998: NDVI relationship to monthly evaporation. *Geophys. Res. Lett.,* **25,** 1753–1756.

Tapley, B. D., S. Bettadpur, M. Watkins, and C. Reigber, 2004: The Gravity Recovery and Climate Experiment: Mission overview and early results. *Geophys. Res. Lett.,* **31,** L09607, doi:10.1029/2004GL019920.

Ummenhofer, C. C., M. H. England, P. C. McIntosh, G. A. Meyers, M. J. Pook, J. S. Risbey, A. S. Gupta, and A. S. Taschetto, 2009: What causes southeast Australia's worst droughts? *Geophys. Res. Lett.,* **36,** L04706, doi:10.1029/2008GL036801.

van Dijk, A. I. J. M., L. J. Renzullo, and M. Rodell, 2011: Use of Gravity Recovery and Climate Experiment terrestrial water storage retrievals to evaluate model estimates by the Australian water resources assessment system. *Water Resour. Res.,* **47,** W11524, doi:10.1029/2011WR010714.

Williams, J. L., III, and R. M. Maxwell, 2011: Propagating subsurface uncertainty to the atmosphere using fully-coupled, stochastic simulations. *J. Hydrometeor.,* **12,** 690–701.

Yang, X., P. L. Smith, T. Yub, and H. Gaob, 2011: Estimating evapotranspiration from terrestrial groundwater-dependent ecosystems using Landsat images. *Int. J. Digital Earth,* **4,** 154–170, doi:10.1080/17538947.2010.491561.

Yeh, P. J.-F., and E. A. B. Eltahir, 2005: Representation of water table dynamics in a land surface scheme. Part I: Model development. *J. Climate,* **18,** 1861–1880.

——, and J. Famiglietti, 2009: Regional groundwater evapotranspiration in Illinois. *J. Hydrometeor.,* **10,** 464–478.

——, S. C. Swenson, J. S. Famiglietti, and M. Rodell, 2006: Remote sensing of groundwater storage changes in Illinois using the Gravity Recovery and Climate Experiment (GRACE). *Water Resour. Res.,* **42,** W12203, doi:10.1029/2006WR005374.

Yi, Y., J. S. Kimball, L. A. Jones, R. H. Reichle, and K. C. McDonald, 2011: Evaluation of MERRA land surface estimates in preparation for the Soil Moisture Active Passive Mission. *J. Climate,* **24,** 3797–3816.

York, J. P., M. Person, W. J. Gutowski, and T. C. Winter, 2002: Putting aquifers into atmospheric simulation models: An example from the Mill Creek Watershed, northeastern Kansas. *Adv. Water Resour.,* **25,** 221–238.

Yuan, H., Y. Dai, Z. Xiao, D. Ji, and W. Shangguan, 2011: Reprocessing the MODIS Leaf Area Index products for land surface and climate modelling. *Remote Sens. Environ.,* **115,** 1171–1187.

Zeng, X., and M. Decker, 2009: Improving the numerical solution of soil moisture-based Richards equation for land models with a deep or shallow water table. *J. Hydrometeor.,* **10,** 308–319.

Zhang, K., J. S. Kimball, R. R. Nemani, and S. W. Running, 2010: A continuous satellite-derived global record of land surface evapotranspiration from 1983 to 2006. *Water Resour. Res.,* **46,** W09522, doi:10.1029/2009WR008800.